

MECHANISTIC CHILLER MODEL DESCRIPTION

Figure 1 shows a schematic and associated pressure-enthalpy diagram of a centrifugal chiller with single stage compression. The refrigerant enters the compressor at state 1 and is assumed to be a saturated vapor. Both the enthalpy and pressure rise as the refrigerant passes through the compressor to a superheated state 2. In the condenser, the refrigerant is cooled and condensed at a constant pressure and is assumed to exit at state 3 as a saturated liquid. It is then expanded at constant enthalpy to the evaporator pressure (state 4). In the development that follows, the chilled water supply and return temperatures, T_{chws} and T_{chwr} , refer to supply and return to load (i.e., from and to the evaporator), while the condenser water supply and return, T_{cws} and T_{cwr} , are to and from the condenser. Each of the components is modeled as follows.

Evaporator

The evaporator is assumed to be a flooded shell-and-tube-type design. Refrigerant boils at the outside of the horizontal tubes and rises out the top. Heat transfer in the evaporator is modeled using an overall conductance and log-mean temperature difference. Three expressions for evaporator heat flow that result from this model and from energy balances on the two fluid streams are

$$Q_e = UA_e LMTD_e \quad (1)$$

$$= m_R (h_1 - h_4) \quad (2)$$

$$= m_{chw} C_{pw} (T_{chwr} - T_{chws}) \quad (3)$$

where

- Q_e = rate of heat transfer to evaporator
- UA_e = overall evaporator conductance
- $LMTD_e$ = evaporator log-mean temperature difference
- m_R = refrigerant mass flow rate
- h_1 = specific enthalpy exiting evaporator
- h_4 = specific enthalpy entering evaporator
- m_{chw} = chilled water flow rate
- C_{pw} = specific heat of water

The log-mean temperature difference and overall conductance are

$$LMTD_e = \frac{(T_{chwr} - T_{chws})}{\ln[(T_{chwr} - T_e)/(T_{chws} - T_e)]} \quad (4)$$

$$UA_e = \frac{A_{e,i}}{(1/h_{e,i} + 1/(r_e h_{e,o}) + R_{e,w})} \quad (5)$$

where

- T_e = refrigerant evaporation temperature
- $A_{e,i}$ = total inside surface area of evaporator tubes
- $h_{e,i}$ = heat transfer coefficient of water flow through evaporator tubes
- $h_{e,o}$ = boiling refrigerant heat transfer coefficient
- r_e = ratio of effective outside (finned) evaporator tube area to inside area
- $R_{e,w}$ = the resistance to heat transfer associated with the tube material, including the fouling factor.

Nucleate boiling is assumed to take place from the evaporator tubes to the pool of re-

refrigerant. Bubbles nucleate and grow from spots on the surface in a thin layer of superheated liquid formed adjacent to the tubes. Much data are available for boiling heat transfer coefficients, but there is no universally accepted correlation. Generally, the heat transfer coefficient for a particular application can be correlated in the form

$$h_{e,o} = a(T_{e,s} - T_e)^b \quad (6)$$

where a and b are empirical constants that depend upon the properties of the refrigerant and the nucleate characteristics of the surface and $T_{e,s}$ is the average tube outside surface temperature. Myers (1952) gives typical results for the heat transfer coefficient of Refrigerant 12 with both plain and finned tubes that are used in this study. An expression for the tube surface temperature, obtained by considering the heat transfer resistance between the water and the outside tube surface is

$$T_{e,s} = \bar{T}_{chw} + \frac{Q_e}{(1/h_{e,i} + R_{e,w})} \quad (7)$$

where \bar{T}_{chw} is the average of the entering and leaving chilled water temperatures.

The chilled water flow through the evaporator tubes is assumed to be turbulent so that the heat transfer coefficient is given as (ASHRAE 1985)

$$h_{e,i} = 0.023(k_w/d_e)Re_e^{0.8}Pr^{0.4} \quad (8)$$

where k_w is the thermal conductivity of water, d_e is the inside tube diameter, Re_e is the Reynolds number associated with water flow in an individual evaporator tube, and Pr is the Prantl number for water.

Condenser

The condenser is also considered to be a horizontal shell-and-tube design. Refrigerant condenses on the outside of the tubes and drains out the bottom. Analogous to the evaporator, the three equations for heat transfer are

$$Q_c = UA_c LMTD_c \quad (9)$$

$$= m_R(h_2 - h_3) \quad (10)$$

$$= m_{cw} C_{pw} (T_{cwr} - T_{cws}) \quad (11)$$

where

h_2 = specific enthalpy entering condenser

h_3 = specific enthalpy exiting condenser

m_{cw} = condenser water flow rate

and

$$LMTD_c = \frac{(T_{cwr} - T_{cws})}{\ln[(T_{cwr} - T_c)/(T_{cws} - T_c)]} \quad (12)$$

$$UA_c = \frac{A_{c,i}}{(1/h_{c,i} + 1/(r_c h_{c,o}) + R_{c,w})} \quad (13)$$

It is not strictly correct to use the refrigerant condensing temperature, T_c , in determining the log-mean temperature difference for the entire condenser. Refrigerant entering the condenser is superheated and is cooled sensibly to the saturation temperature at constant pressure prior to condensation. During this process, the heat transfer coefficient is lower

and the temperature difference higher than during condensation. These considerations provide some justification for using a single condenser temperature along with the condensing heat transfer coefficient in the model.

Theoretical expressions for determining the heat transfer coefficients for laminar film condensation of pure vapors on plates and tubes were first developed by Nusselt. The average heat transfer coefficient associated with a vapor condensing on N horizontal tubes is estimated from (Stoecker 1982):

$$h_{c,o} = 0.725 \left[\frac{k_f^3 (\rho_f - \rho_v)^2 g h_{fg}}{N d_c \mu_f (T_c - T_{c,s})} \right]^{0.25} \quad (14)$$

where

- k_f = conductivity of the liquid refrigerant
- h_{fg} = heat of vaporization of the refrigerant
- g = gravitational acceleration
- ρ_f = density of saturated liquid
- ρ_v = density of saturated vapor
- d_c = condenser tube diameter
- μ_f = viscosity of saturated liquid
- $T_{c,s}$ = average tube outside surface temperature

The vapor density is usually small compared to the liquid density and may be neglected. Analogous to the evaporator analysis, the tube surface temperature is

$$T_{c,s} = \bar{T}_{cw} + \frac{Q_c}{(1/h_{c,i} + R_{c,w})} \quad (15)$$

where \bar{T}_{cw} is the average condenser water temperature.

The correlation for turbulent flow in tubes, Equation 8, is applicable to a condenser tube and is used for evaluating the water-side heat transfer coefficient for the condenser, h_{ci} .

Compressor

One approach to modeling the performance of the compressor is to use performance curves based on the manufacturer's data. Davis (1974) presents a method of correlating the data that reduces the family of compressor head characteristics to a single curve of dimensionless head versus a dimensionless flow. A limitation associated with this approach is that complete performance data are not always readily available or they are presented in such a way as to be specific to the refrigerant employed.

The model developed in this study relies on relationships that are commonly used in the design of centrifugal compressors. It employs fundamental mass, momentum, and energy balances and empirical correlations that are representative of well-designed centrifugal compressors.

Ferguson (1963) provides the background for much of the presentation to follow. Figure 2 shows a cross section of the impeller of a centrifugal compressor, showing a single blade with pertinent dimensions and velocities. The impeller rotates with an angular velocity ω , having a tip speed equal to u_x . The refrigerant vapor exits the impeller with a relative velocity $V_{x,r}$ and an absolute velocity V_x . The components of velocity tangential and normal to the impeller wheel are denoted as $V_{x,t}$ and $V_{x,n}$.

Neglecting the angular momentum of the incoming refrigerant and the frictional torque, a momentum balance on the impeller gives an expression for the required work input per unit mass flow.

$$W = \omega V_{x,t} r = u_x V_{x,t} = \mu_x u_x^2 \quad (16)$$

where the work coefficient, μ_x , is defined as the ratio of the tangential component of the fluid velocity to the impeller tip speed.

$$\mu_x = \frac{V_{x,t}}{u_x} \quad (17)$$

If the velocity of the fluid relative to the impeller, $V_{x,r}$, exits tangential to the blade (i.e., no slippage), then the theoretical work coefficient determined from the vector diagram of Figure 2 is

$$\begin{aligned} \mu_{x,th} &= \frac{u_x - V_{x,n} \cot(\beta)}{u_x} \\ &= 1 - \phi_x \cot(\beta) \end{aligned} \quad (18)$$

The dimensionless flow coefficient, ϕ_x , is the ratio of the fluid velocity normal to the impeller to the impeller tip speed.

$$\phi_x = \frac{V_{x,n}}{u_x} = \frac{m R v_x}{A_x u_x} \quad (19)$$

where A_x is the effective exit flow area of the impeller and v_x is the exiting vapor specific volume.

In reality, slippage and nonuniform velocity profiles at the impeller exit limit the accuracy of this formulation. Wiesner (1959,1960) has correlated the real performance of centrifugal compressors with vaneless diffusers. His results are presented as curves of polytropic efficiency, η_{pol} , and polytropic work coefficient, μ_{pol} , versus the dimensionless flow coefficient, ϕ_x , where,

$$\eta_{pol} = \frac{W_{pol}}{W} \quad (20)$$

$$\mu_{pol} = \frac{W_{pol}}{u_x^2} \quad (21)$$

The polytropic work, W_{pol} , is the work required for a reversible polytropic process occurring between the actual inlet and outlet states. A polytropic process satisfies

$$Pv^n = \text{constant} \quad (22)$$

where the polytropic coefficient, n , is determined by the actual initial and end states from

$$n = \frac{v_2}{v_1} \ln \left[\frac{P_2}{P_1} \right] \quad (23)$$

Since there is an increase of entropy in the actual irreversible compressor, there must be a reversible heat input to the reversible compressor for the end states to be the same. The polytropic work is given by

$$W_{pol} = \int v dP = P_1 v_1 \frac{n}{n-1} \left[(P_2/P_1)^{(n-1)/n} - 1 \right] \quad (24)$$

The stage work coefficient, μ_x , is determined from the polytropic coefficient and efficiency as

$$\mu_x = \frac{\mu_{pol}}{\eta_{pol}} \quad (25)$$

Wiesner's results for μ_{pol} are a series of straight lines that can be represented by

$$\mu_{pol} = 0.69 (1 - \phi_x \cot(\beta)) = 0.69 \mu_{x,th} \quad (26)$$

The polytropic efficiency results of Wiesner are presented as curves of relative efficiency versus the dimensionless flow coefficient, ϕ_x , for different rotational Mach numbers, M_o , where

$$M_o = \frac{u_x}{a_o} \quad (27)$$

and a_o is the sonic velocity in the refrigerant at the impeller inlet conditions. The following equation provides a good fit to the graphical data of Wiesner.

$$\frac{\eta_{pol}}{\eta_{ref}} = [1 + a(1.1 - M_o)][1 - \exp(\phi_x(b\phi_x^2 + c\phi_x + d))] \quad (28)$$

The reference polytropic efficiency, η_{ref} , is the peak value associated with a reference rotational Mach number, M_{ref} , of 1.1. It is typically in the range of 0.80 to 0.85. The empirical constants (a, b, c, d) that provide a good match to Wiesner's data are 0.109, 58.5, -6.0, and -18.8, respectively. Wiesner also presents a correction factor for polytropic efficiencies due to differences in Reynolds numbers associated with the use of different refrigerants. This effect is relatively small and is negligible for the refrigerants considered in this study (R-500, R-22, and R-12).

In order to evaluate the flow coefficient using Equation 19, it is necessary to determine the specific volume of the refrigerant at the exit of the impeller. Most of the entropy rise associated with the compression process occurs within the diffuser. For this reason, the entropy at the impeller exit is assumed to be equal to the entropy at the inlet.

$$s_x = s_1 \quad (29)$$

The additional property necessary to define the state at the impeller outlet is determined from an energy balance on the diffuser. Assuming that the kinetic energy exiting the diffuser is small compared to that at the diffuser inlet, the incoming enthalpy is

$$h_x = h_2 - \frac{v_x^2}{2} \quad (30)$$

From an energy balance on the impeller and Equation 16,

$$h_2 = h_1 + \mu_x u_x^2 \quad (31)$$

So,

$$h_x = h_1 + \mu_x u_x^2 - \frac{v_x^2}{2} \quad (32)$$

The absolute refrigerant velocity at the impeller exit, V_x , is determined from the normal and tangential components (Figure 2), such that

$$V_x^2 = v_{x,n}^2 + v_{x,t}^2 = u_x^2(\phi_x^2 + \mu_x^2) \quad (33)$$

Thus the exit impeller enthalpy is

$$h_x = h_1 + u_x^2 (\mu_x - 0.5\mu_x^2 - 0.5\phi_x^2) \quad (34)$$

The thermal expansion device is assumed to modulate the refrigerant flow so that a saturated vapor state is maintained at the compressor inlet. The entering and exiting enthalpy of the expansion device are assumed to be equal.

$$h_4 = h_3 \quad (35)$$

Finally, the power input to the motor driving the compressor is calculated as

$$P = \frac{m_R(h_2 - h_1)}{\eta_m} \quad (36)$$

where η_m is the overall efficiency associated with the motor and gearbox if present. The heat losses associated with these inefficiencies are not considered to be useful.

The model, as defined through Equations 1-36, requires properties of the refrigerant at various states. A computer program developed from the equations given by Downing (1981) was used to evaluate thermodynamic properties of the refrigerants at any state. Additionally, curve fits were developed for viscosity and conductivity at saturated liquid conditions for refrigerants considered in this study. The sonic velocity associated with the vapor refrigerant exhibits very little variation over a wide range of temperatures. It was assumed to be constant evaluated at 50F.

SOLUTION OF THE EQUATIONS

For a given chiller design, there are five independent input variables that define the chiller performance through the equations presented in the previous section. It is possible to solve these equations in different ways depending upon the desired inputs and outputs. Most commonly, the independent variables controlling the compressor performance would be the entering chilled and condenser water temperatures and flow rates and the chilled water setpoint. In this case, the primary outputs would be the compressor power requirement and speed. Alternatively, it is possible to specify the compressor speed as an input, in which case the leaving chilled water temperature and power requirement are outputs. Other possibilities include specifying the leaving in place of the entering condenser water temperature or the power consumption.

For a single-stage compressor, with a specified chilled water setpoint and entering or leaving condenser water temperature, the equations are solved in two steps:

1. Given the chilled water entering flow rate and temperature and the set-point, determine the evaporator's refrigerant temperature by iteratively solving Equations 1 and 3-8. This can be accomplished with Newton's method applied to the function.

$$UA_e LMTD_e - m_{chw} C_{pw} (T_{chwr} - T_{chws}) = 0 \quad (37)$$

2. The solution of the remaining set of equations can be reduced to finding the solution of three functions with three unknowns using Newton's method. The three unknowns are T_c , u_x , and ϕ_x , while the three functions are

$$UA_c LMTD_c - m_{cw} C_{pw} (T_{cwr} - T_{cws}) = 0 \quad (38)$$

$$\phi_x - \frac{m_R v_x}{A_x u_x} = 0 \quad (39)$$

$$(h_2 - h_1) - \frac{W_{pol}}{\eta_{pol}} = 0 \quad (40)$$

For given values of the unknowns, each of the terms in the above equations are uniquely defined with Equations 2, 9-35 and property data.

The analysis is complicated a bit further if two stage compression is considered. In this case, the energy and momentum balances are applied to both compression stages. In the absence of an economizer, the outlet from the first stage is the inlet the second.

Most multistage centrifugal chillers utilize an economizer. For a two-stage compressor, refrigerant exiting the condenser is expanded to the intermediate pressure between compression stages and enters a flash tank. Saturated refrigerant vapor is removed from the flash tank, mixed with the outlet stream from the first stage, and fed to the second-stage compressor. Liquid refrigerant from the flash tank is expanded to the evaporator pressure. In order to include an economizer in the analysis, mass and energy balances are applied to the economizer to determine the additional states and refrigerant flow rates.

In the solution of equations for two-stage compression, two additional unknowns are the intermediate pressure and the flow coefficient for the second stage. Equations 39 and 40 apply to first stage and an analogous two additional equations are used for the second stage.

The maximum cooling capacity of a chiller is limited by several factors. For instance, it may be controlled by the maximum allowable power input to the motor or the maximum rotational speed. Alternatively, there may be a lower limit on the refrigerant temperature in order to avoid localized ice formation within the evaporator or an upper limit on the condenser pressure. In any of these situations, the model can be adapted to determine the maximum capacity and associated power input and compressor speed. The D/FW chiller capacity is primarily limited by the power input to the motor. In this case, the equations are solved so that power is an input and cooling capacity is output. Equations 37-40 are solved concurrently, rather than separately in this situation.

PARAMETER ESTIMATION AND COMPARISON WITH MEASUREMENTS

The D/FW chiller has two-stage compression with an economizer. Many of the parameters characterizing this design were available from the manufacturer and are presented in Table 1. Additional parameters necessary for evaluating the chiller performance were determined by regression using measurements from the D/FW airport. The data used in the regression were randomly selected from one-minute measurements for two different time periods in August and October to give a range of conditions.

The ratios of the effective outside finned tube area to the inside area for both the evaporator and condenser were unknown. Sufficient data were available to estimate these ratios from a regression analysis. The saturation temperatures were estimated from compressor suction and discharge pressure measurements using refrigerant property data for R-500. Good agreement between the model and the saturation temperatures is obtained for values of r_e and r_c of 3.1 and 3.2. The tubing used in both the evaporator and condenser is identical. It is therefore reassuring to note the closeness in the values of r_e and r_c determined by regression.

The efficiency of the electric motor driving the compressor is approximately 95%. Additionally, there is significant energy loss in the gearbox between the motor and the compressor. At maximum loading of 5000 hp (3729 kW), the energy loss is approximately 200 hp (149 kW), resulting in an overall efficiency of about 91%.

There are three additional unknown parameters concerning the compressor that are necessary in order to analyze the chiller performance: (1) the impeller blade angle, β ; (2) the impeller exit flow area, A_x ; and (3) the reference polytropic efficiency, η_{ref} . Estimates of these parameters were obtained from the D/FW plant personnel and the literature as follows.

From a photograph of a centrifugal compressor impeller available from the D/FW plant personnel, the blade angle appears to be approximately 30° . The impeller width at the exit is between 2 and 3 inches. This gives an impeller exit area of between 1.2 and 1.8 square feet. Wiesner's (1960) curves of polytropic efficiency, derived from measurements of several centrifugal compressors operating with R-500, R-22, or R-12, give a relative polytropic efficiency of about 0.82.

In order to fine-tune these estimates, a regression analysis was applied to the centrifugal compressor. The power input to the compressor was estimated from measurements of the electrical consumption of the motor and the estimated motor plus gearbox efficiency. The unknown compressor parameters were determined by minimizing the sum of squares of the differences between measurements and model results from both compressor power and speed. Table 2 gives the parameter values determined from the regression analysis. They are surprisingly close to the original estimates.

Figures 3-6 show comparisons between measurements and predictions of the complete model for refrigerant temperatures in the evaporator and condenser and the compressor power and speed. The best predictions are of the power consumption and the evaporator temperature. The estimates of the condenser temperature and compressor rpm are not quite as good. There appears to be a slight bias in the comparisons. The model tends to underestimate power consumption and speed at low values. One possibility is that the motor and gearbox efficiencies are lower at lower speeds and loadings. The model assumes a fixed overall efficiency for these components at all conditions. Another possibility is that the compressor polytropic efficiency may fall off more significantly at low loads than the Wiesner data exhibit.

The D/FW measurements were originally recorded on magnetic tape at one minute intervals during normal operation. For the comparisons of Figures 3-6, the data were selected randomly. Part of the variability in these results may be a result of unsteady conditions. As another test of the accuracy of the model, controlled tests were performed on the chiller and compared with model predictions for a range of conditions. The conditions for all measurements were stabilized for at least 15 minutes. Both the chilled and condenser water flow rates were held relatively constant. The results of the comparisons are summarized in Table 3. Once again, the estimates of power consumption are better than estimates of compressor speed. The rms of the differences is 84 kW for power and 140 rpm for compressor speed. The relative error of the power consumption estimates is larger at low loads, due in part to the much larger uncertainty in the load evaluation at this condition. Errors in measurements of chilled water temperature differences, used to determine the chiller load, have a much more significant effect when the differences are small.

SURGE PREDICTIONS

The operating temperature and pressure of the refrigerant in the evaporator are determined by the chilled water load, the water flow rate, and the chilled water setpoint. Similarly, the condensing pressure depends upon the total heat rejection and the condenser's water stream conditions. A surge condition occurs when the compressor is unable to develop a discharge pressure sufficient to satisfy the condenser requirements. This results in an unstable mode of operation in which the total flow in the compressor oscillates. During the surge cycle, the compressor travels up and down its pressure-flow characteristic curve.

An additional mathematical characteristic of the surge condition is that it first develops at a point of zero slope of the discharge pressure versus flow relationship. This condition also corresponds to a point of zero slope of the compressor speed versus chiller loading characteristic. Figure 7 shows results of the model for required compressor speed versus loading for conditions at which an estimate of the actual surge point was known. The modeled surge point occurs at the minimum speed. To the left of this point, the model predicts that the compressor speed increases with decreasing load. The "known" surge point occurs at about 2900 rpm and 1340 tons (4.7 MW). The minimum modeled compressor speed is 2700 rpm and is relatively close to this value, but the load associated with this speed (450 tons [1.6 MW]) is significantly lower. It is difficult to predict the load associated with the development of surge. As evident in Figure 7, the chiller cooling capacity is extremely sensitive to compressor speed near the surge point. The determination of the onset of surge requires a subjective decision. The surge point cannot be measured directly. In this work, the approach used in modeling surge is to first determine the minimum possible compressor speed for any given set of conditions. The point at which surge develops is then assumed to

occur at 50 rpm greater than this minimum. At this point, Figure 7 indicates that there is essentially a linear relationship between speed and chiller capacity.

The chiller model is easily adapted to determine the compressor speed at which surge first occurs for a given set of chilled and condenser water conditions. An optimization routine, such as golden section search, is used to calculate the minimum compressor speed as a function of chiller loading.

Figure 8 shows a comparison of compressor speeds at which surge develops for the model and D/FW data as a function of the temperature difference between the leaving condenser and evaporator water flow streams. The predictions are within about 50 rpm of the measurements.

PERFORMANCE CHARACTERISTICS OF THE D/FW CHILLER

The mechanistic model matches experimental data and can be used with confidence to develop a complete performance map of the chiller. Figures 9 and 10 show the D/FW chiller performance expressed in difference ways. Figure 9 gives capacity as a function of compressor speed and the temperature difference between the leaving water streams. Within the constraints imposed by surge and the maximum capacity, the cooling output of the chiller is nearly linear with compressor speed at a fixed temperature difference. With increasing temperature differences, the range in which capacity may be controlled is reduced. The chiller cannot operate above a temperature difference where the surge and maximum capacity lines would intersect.

Figure 10 shows the power requirements as a function of the load and the water temperature difference. Although it is difficult to distinguish, results are presented for two different chilled water setpoints of 40F and 50F (same temperature differences). It is clear that the performance is almost totally independent of the individual leaving chilled and condenser water temperatures, depending primarily upon their difference. This is a useful result in the development of a simple empirical correlation to chiller performance data.

Figure 11 shows the chiller coefficient of performance (COP) plotted versus chiller load for different leaving water temperature differences. Consistent with the expression for Carnot efficiency, the chiller COP increases with decreasing temperature difference between the condenser and evaporator streams. The COP reaches a maximum at low chiller loads. This peak occurs as a result of trade-offs between increasing heat transfer efficiencies due to decreased water to refrigerant temperature differences in the evaporator and condenser and the decreased polytropic efficiencies of the compressor that occur at low refrigerant flow rates. The peak COP moves to lower loads at lower temperature differences. It occurs at part-loads of between 35% to 70% of the chiller design capacity of 5500 tons (19.3 MW).

Figure 12 shows the effect of chilled and condenser water flow rates on the COP of the chiller. In the normal operating range of this chiller, the effect of variations in either flow rate on the overall performance of the chiller is relatively small when the results are presented in terms of leaving water temperatures. It is interesting to note that reducing the evaporator flow shows an improvement in the performance. This results from the characterization of the performance in terms of the load and leaving chilled water temperature. For a given load and chilled water setpoint, a lower flow gives a higher chilled water return. Assuming that this dominates over the reduced heat transfer coefficient effect, the evaporation temperature rises and the performance improves. In practice, the chilled water return temperature is constrained by comfort considerations at the distribution points to the load.

The chiller model is also useful for studying the effect of different refrigerants on the overall chiller performance. Figures 13 and 14 show COP as a function of load at different leaving water conditions for R-500, R-22, and R-12. The D/FW chiller as installed was charged with R-22. Upon retrofit with a variable speed drive, the refrigerant was changed to R-500. Since the maximum chiller load is generally less than about 5500 tons (19.3 MW), Figures 13 and 14 indicate that this was a relatively good choice. Overall, R-22 does well at very high loads, both R-12 and R-500 are good at loads near 5500 tons (19.3 MW), and R-12 is a clear choice at lower loads. It appears that R-12 may be a better choice than R-500. This type of information is of interest to a plant manager contemplating a change of refrigerants.

CONCLUSIONS

A detailed mechanistic model of a variable-speed centrifugal chiller has been developed. The model requires only design parameters and the operating conditions in order to estimate the power requirement. The model also is capable of estimating the compressor speed at which surge develops or the maximum chiller cooling capacity at a given power input or speed. Results of the model compare favorably with measurements from the D/FW airport for both power requirement and the speed associated with the onset of surge. The mechanistic model was used to study the performance characteristics of the D/FW chiller. The best chiller performance occurs at part-loads of between 35% and 70% of the design capacity of 5500 tons (19.3 MW), depending upon the temperature difference between the leaving water streams. The power requirement of a particular chiller depends primarily upon two variables: the chilled water load and the temperature difference between the leaving condenser and chilled water streams. This is a useful result for correlating performance data for centrifugal chillers. The use of different refrigerants was also investigated. The use of R-12 shows about a 5% improvement over the current choice of R-500 at part-load conditions.

REFERENCES

- ASHRAE. 1985. ASHRAE Handbook-Fundamentals, Atlanta.
- Bullock, C.E. 1984. "Dynamic simulation models for commercial air conditioning and heat pump systems." Georgia Institute of Technology. Proceedings of the Workshop on HVAC Controls Modeling and Simulation.
- Davis, F.T. and Corripio, A.B. 1974. "Dynamic simulation of variable speed centrifugal compressors," Instrumentation in the Chemical and Petroleum Industries, Vol. 10, ISA, Pittsburgh, PA.
- Downing, R.C., Refrigerant Equations, Dupont Company.
- Ferguson. 1963. The centrifugal compressor stage, London: Butterworth and Company.
- Myers, J.E. and Katz. 1952. "Boiling coefficients outside horizontal plain and finned tubes," Refrigeration Engineering, vol. 60, No. 1, p. 56.
- Wiesner, F.J. and Caswell, H.E. 1959. "How refrigerant properties affect impeller dimensions," ASHRAE Journal (October).
- Wiesner, F.J. 1960. "Practical stage correlations for centrifugal compressors", ASME Transactions, Houston: Gas Turbine Power and Hydraulic Conference, Paper 60-HYD-17.
- Stoecker, W.F. 1971. Proposed procedures for simulating the performance of components and systems for energy calculations, 2d Ed. New York: ASHRAE.
- Stoecker, W.F. 1982. Refrigeration and air conditioning, 2d Ed., New York: McGraw-Hill.

TABLE 1

Known D/FW Chiller Parameters

<u>Description</u>	<u>Value</u>	<u>Units</u>
Effective evaporator internal tube surface area	11,300	square feet
Number of evaporator tubes	3,560	
Number evaporator tube passes	3	
Evaporator tube length	22	feet
Tube inside diameter (evaporator & condenser)	0.75	inches
Effective condenser internal tube	14,800	square feet
Number of condenser tubes	3,349	
Number of condenser tube passes	1	
Condenser tube length	30	feet
Diameter of compressor impellers	2.33	feet

TABLE 2
Compressor Parameters Determined from Regression

<u>Parameter</u>	<u>Value</u>	<u>Units</u>
β	27.2	degrees
A_x	1.53	square feet
η_{ref}	0.814	

TABLE 3
Comparisons with Controlled Tests

<u>Load (Tons)</u>	<u>T_{chws}(F)</u>	<u>T_{cwr}(F)</u>	<u>Power(kW)</u>		<u>Speed(rpm)</u>	
			<u>Data</u>	<u>Model</u>	<u>Data</u>	<u>Model</u>
1375	40	57	364	302	2350	2177
2475	41	64	650	755	2600	2695
2800	40	69	1010	1082	3100	2992
2750	40	79	1411	1421	3400	3258
2710	40	64	805	867	1400	1563
1355	50	57	126	134	1400	1562
5420	40	69	2416	2248	3600	3572
5460	40	76	2736	2774	3700	3755
5420	40	86	3580	3519	3900	3971
2690	50	62	415	461	2700	2498
2750	50	69	610	689	2700	2497
2730	50	82	1299	1154	3200	2955
4065	50	64	940	864	2650	2624
4065	50	75	1316	1391	3000	3004

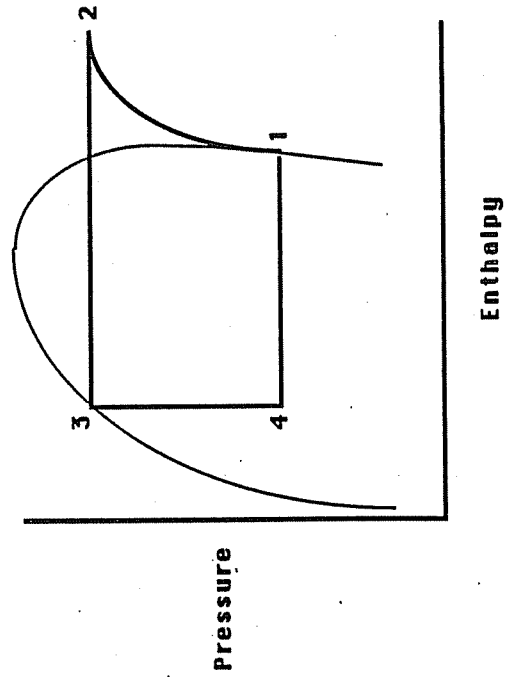
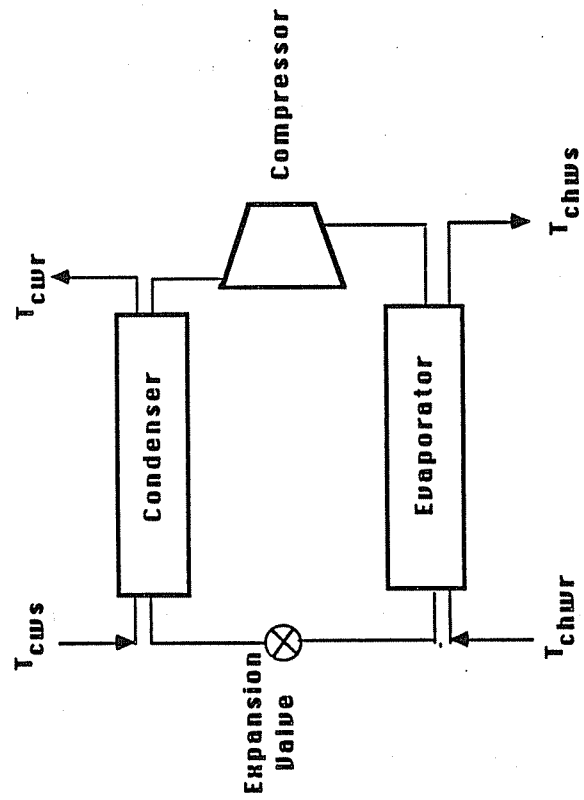
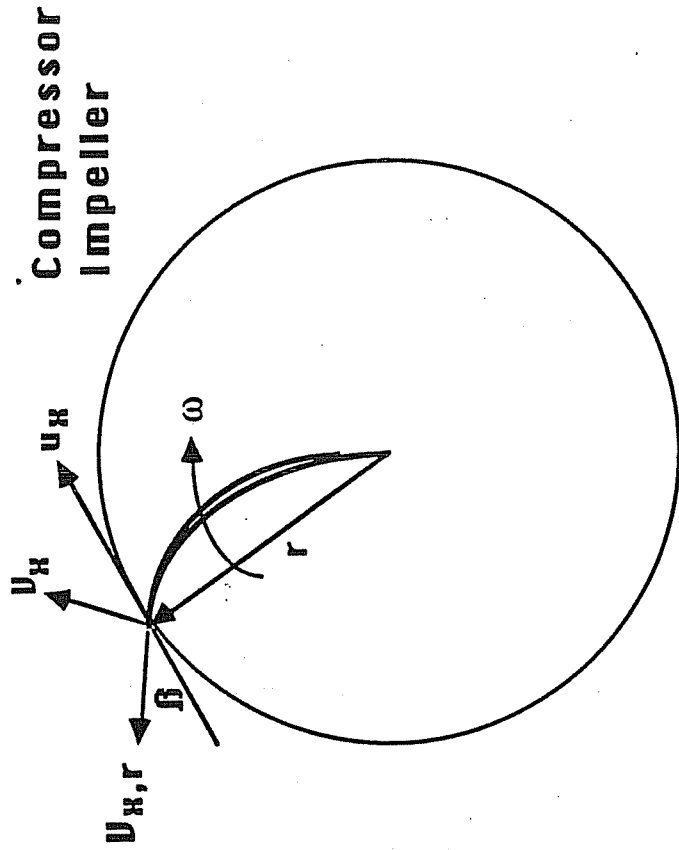


Figure 1. Schematic and pressure-enthalpy diagram for a single-stage chiller



Velocity Vectors

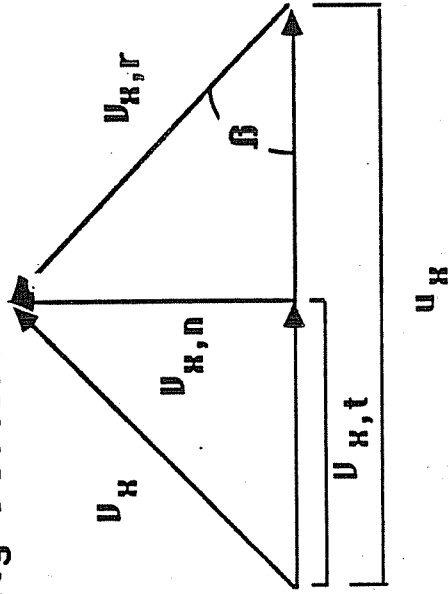


Figure 2. Velocity components for refrigerant exiting a compressor impeller

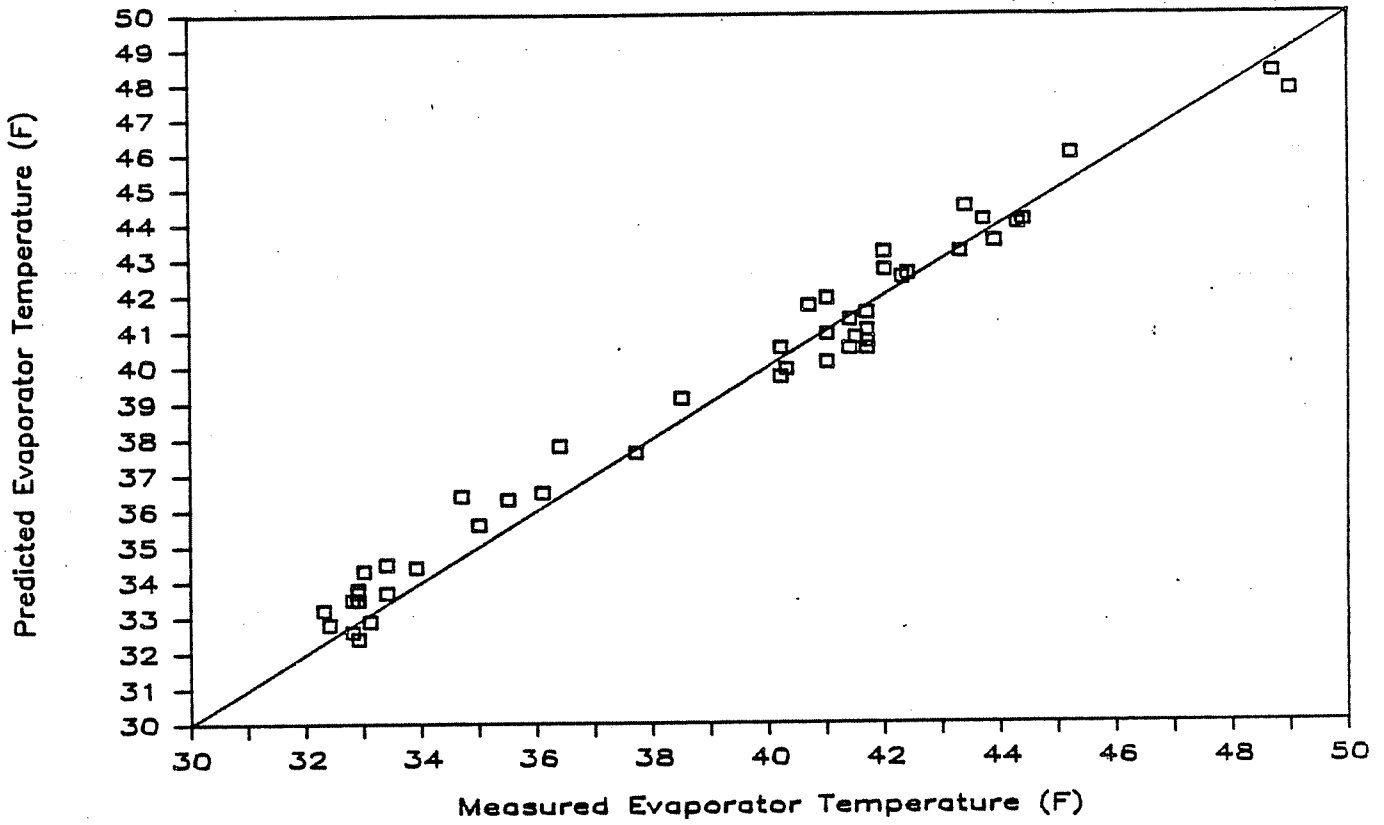


Figure 3. Comparison of modeled evaporator temperatures with D/FW measurements

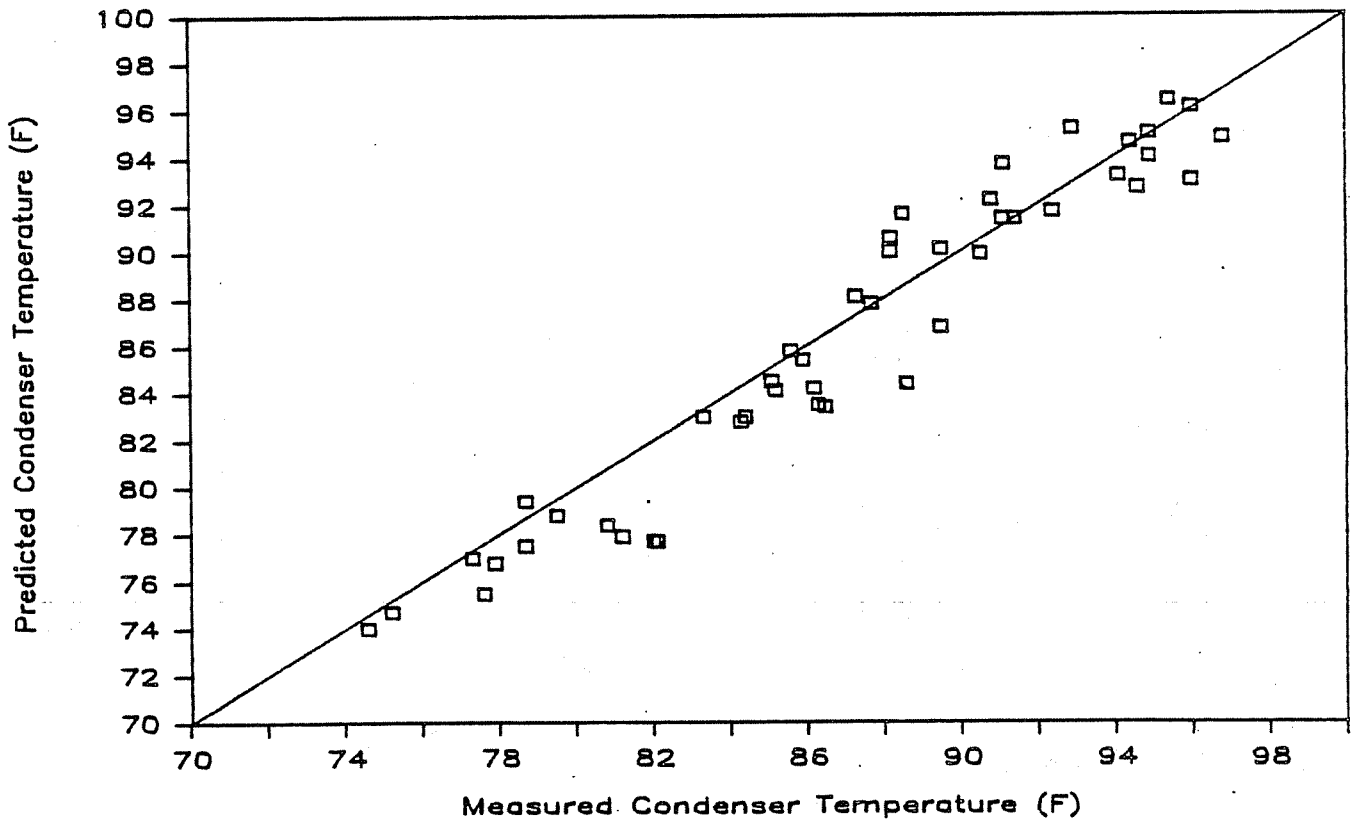


Figure 4. Comparison of modeled condenser temperatures with D/FW measurements

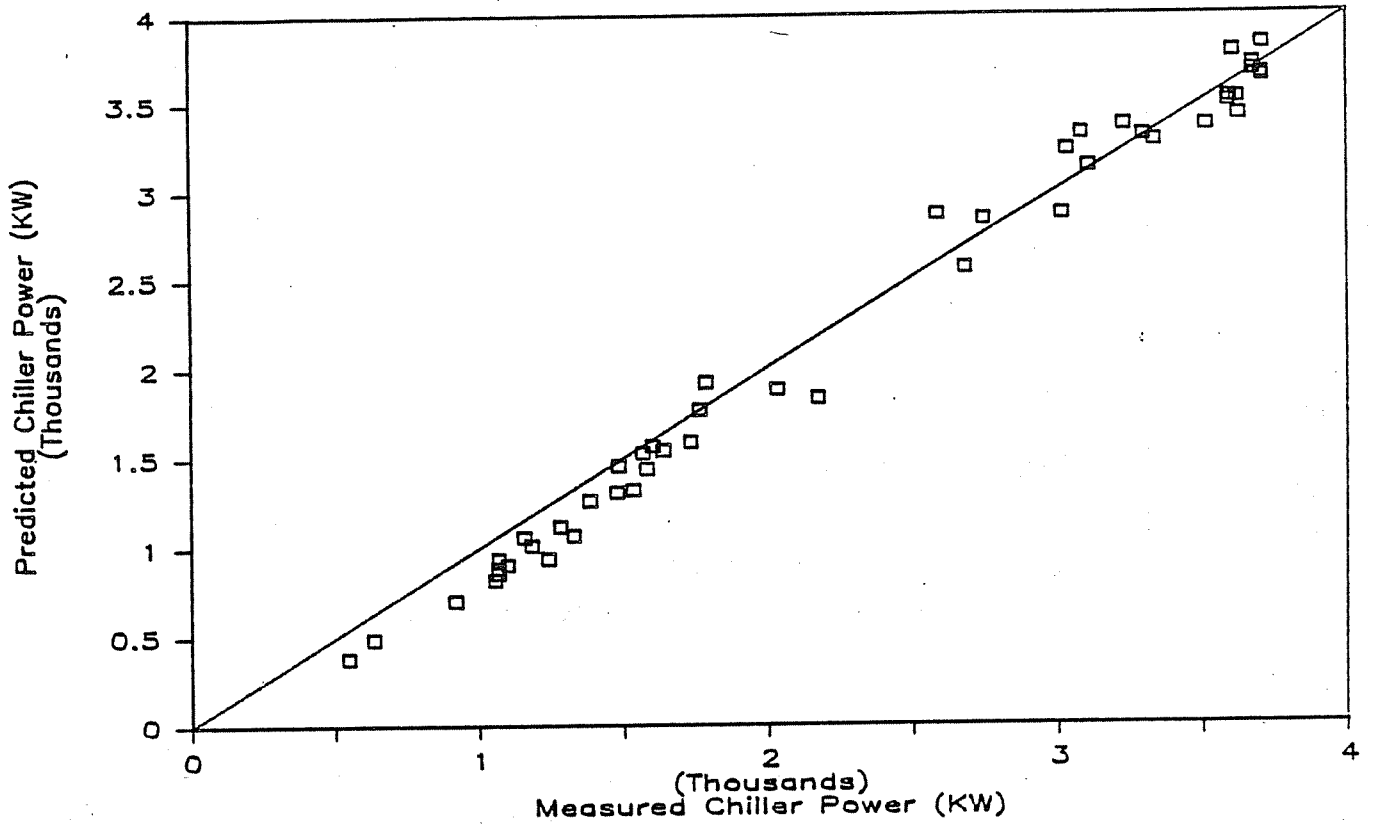


Figure 5. Comparison of modeled power consumption with D/FW measurements

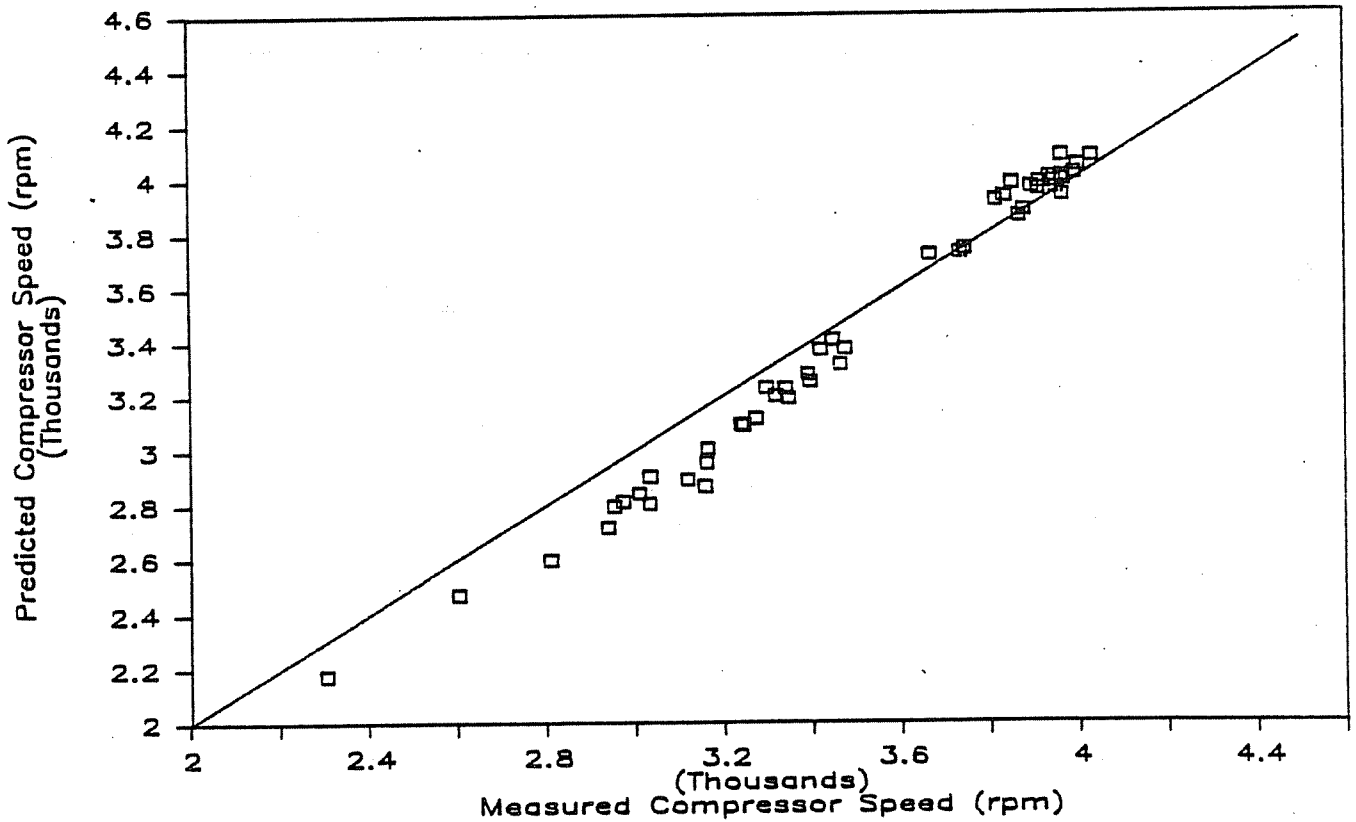


Figure 6. Comparison of modeled compressor speed with D/FW measurements

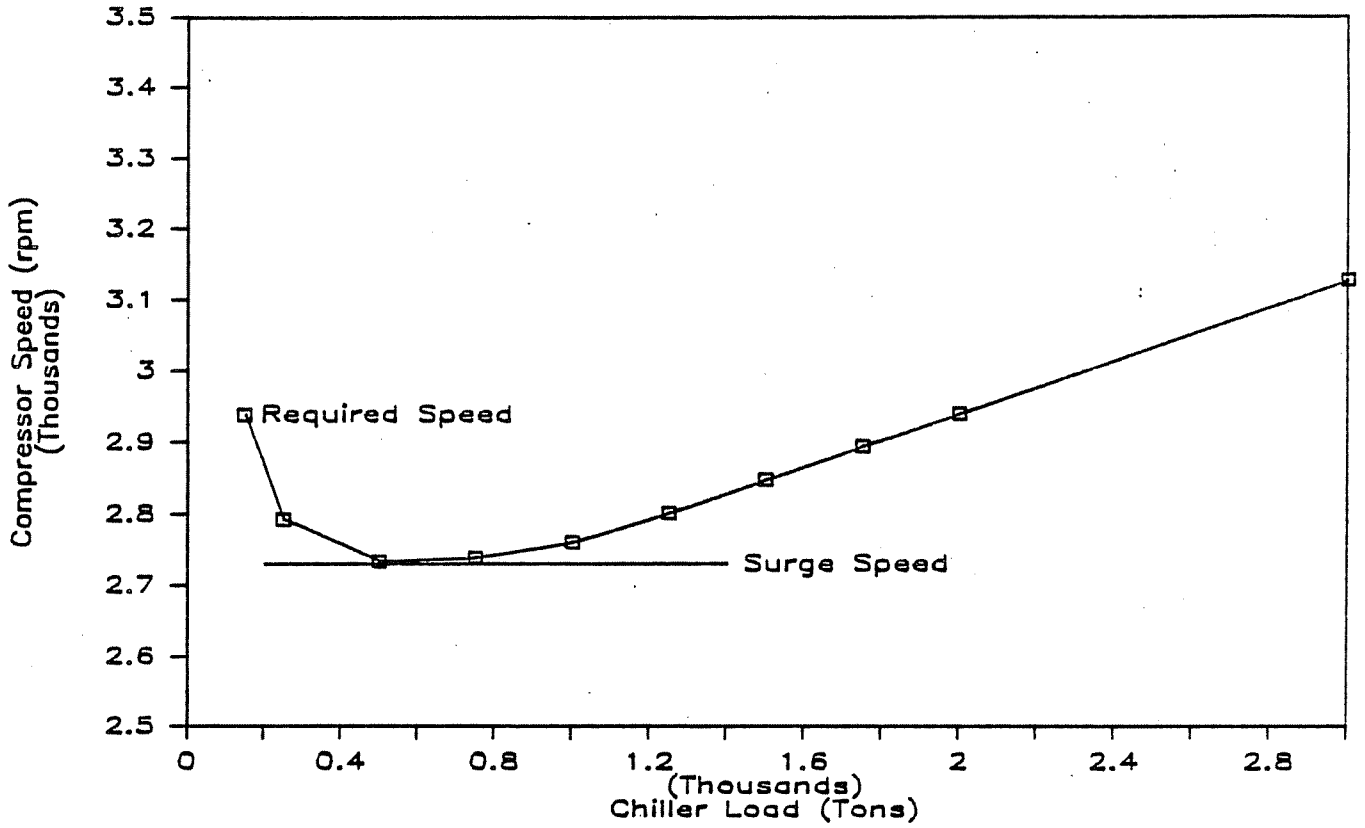


Figure 7. Modeled compressor speed vs. load requirement

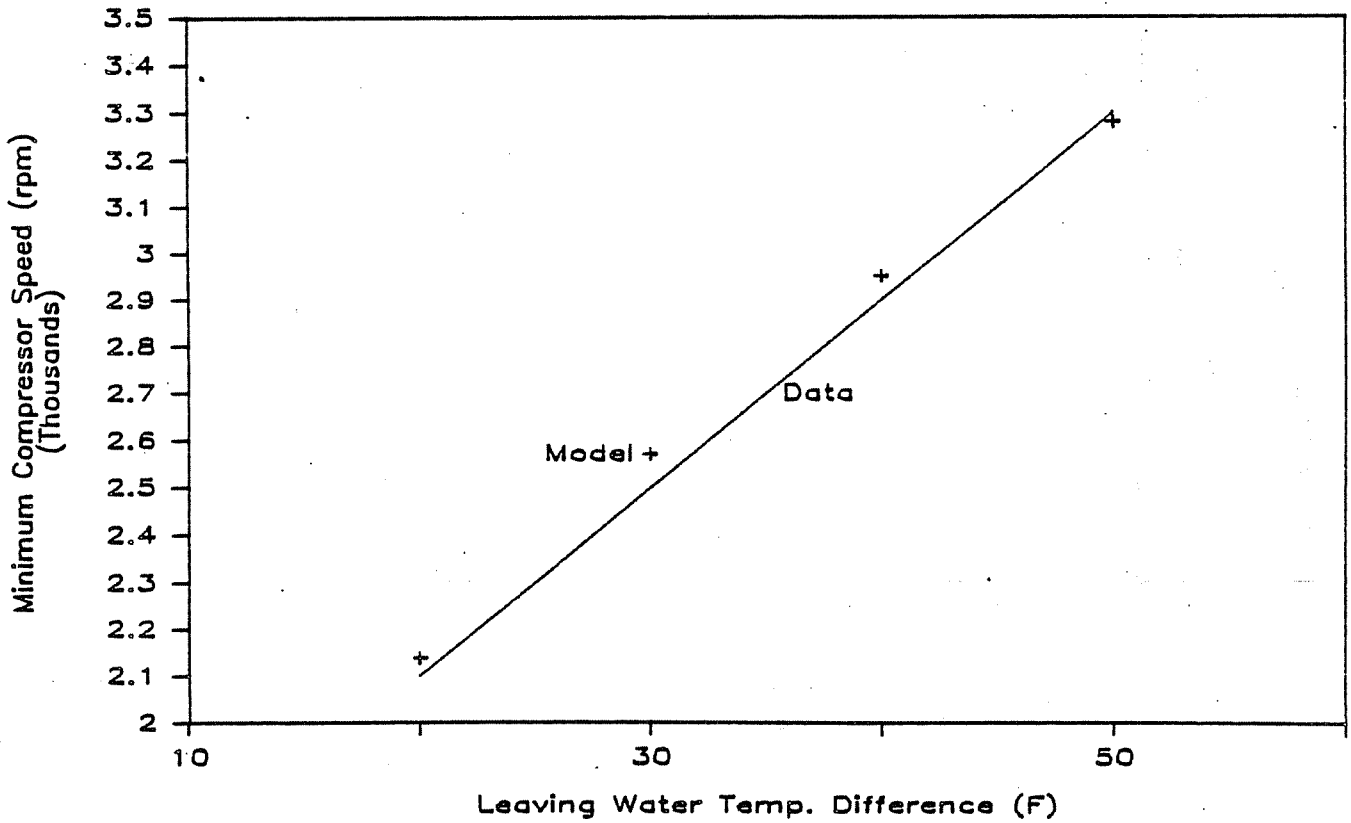


Figure 8. Comparison of modeled surge speed with D/FW data

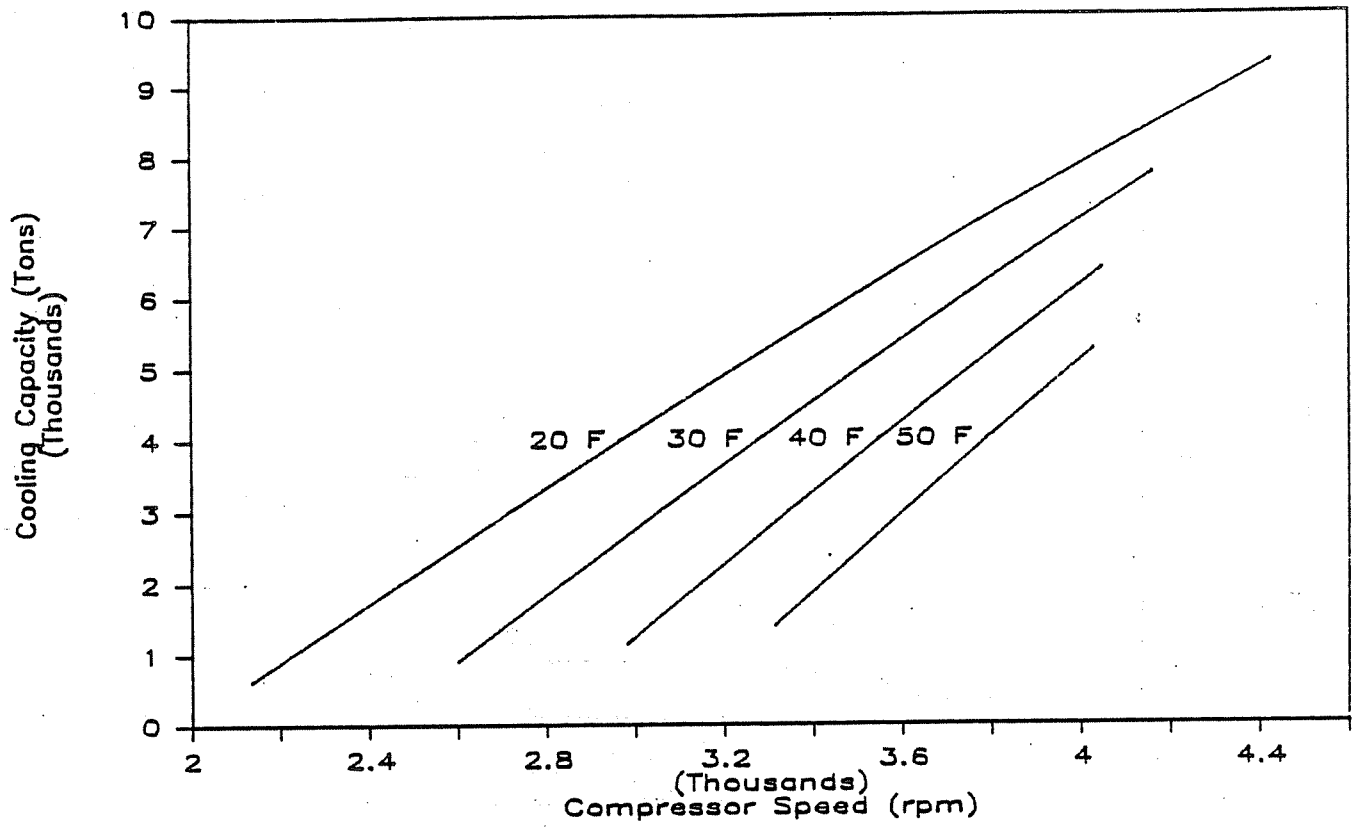


Figure 9. Modeled D/FW chiller capacity vs. compressor speed and leaving water temperature difference

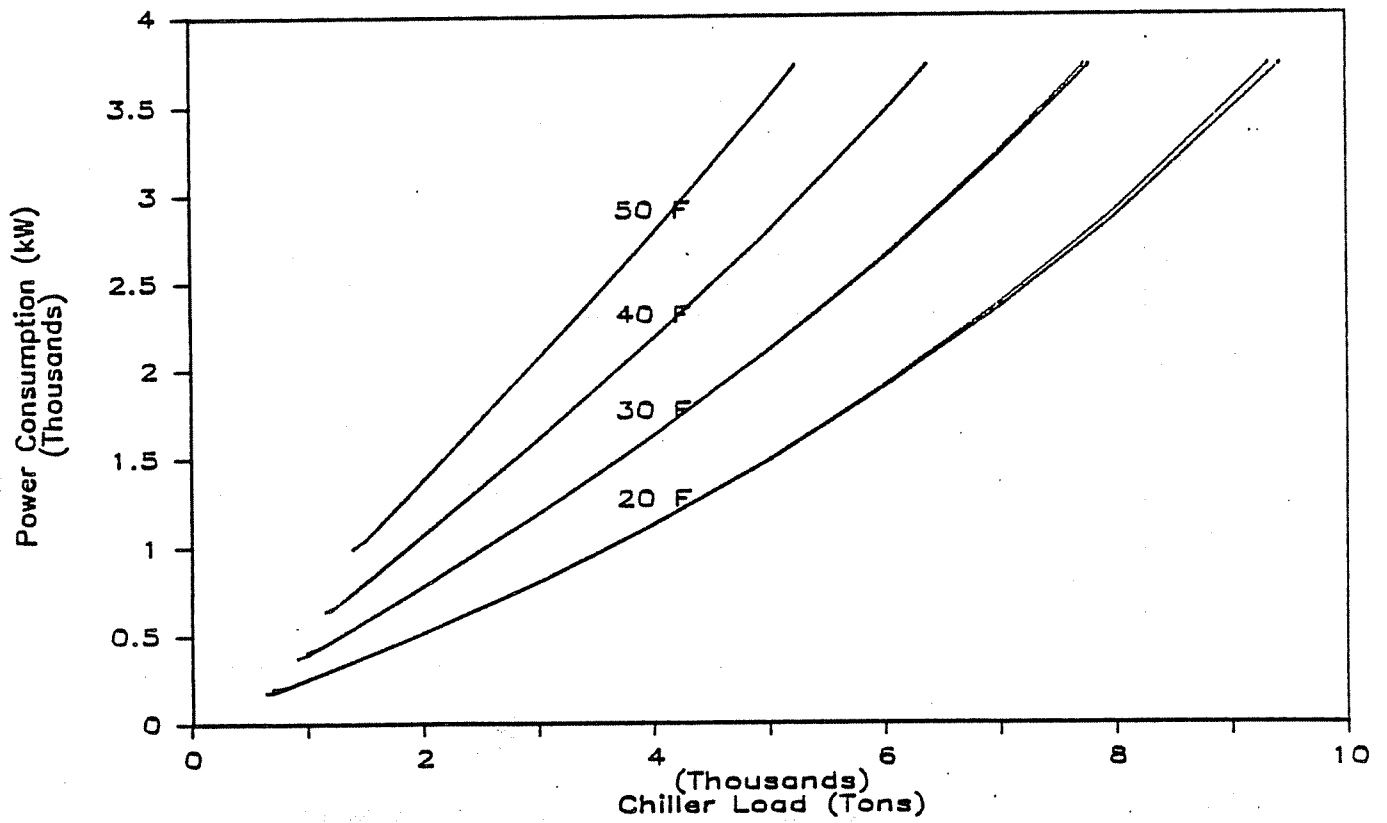


Figure 10. Modeled D/FW chiller power consumption vs. load requirement and leaving water temperature difference

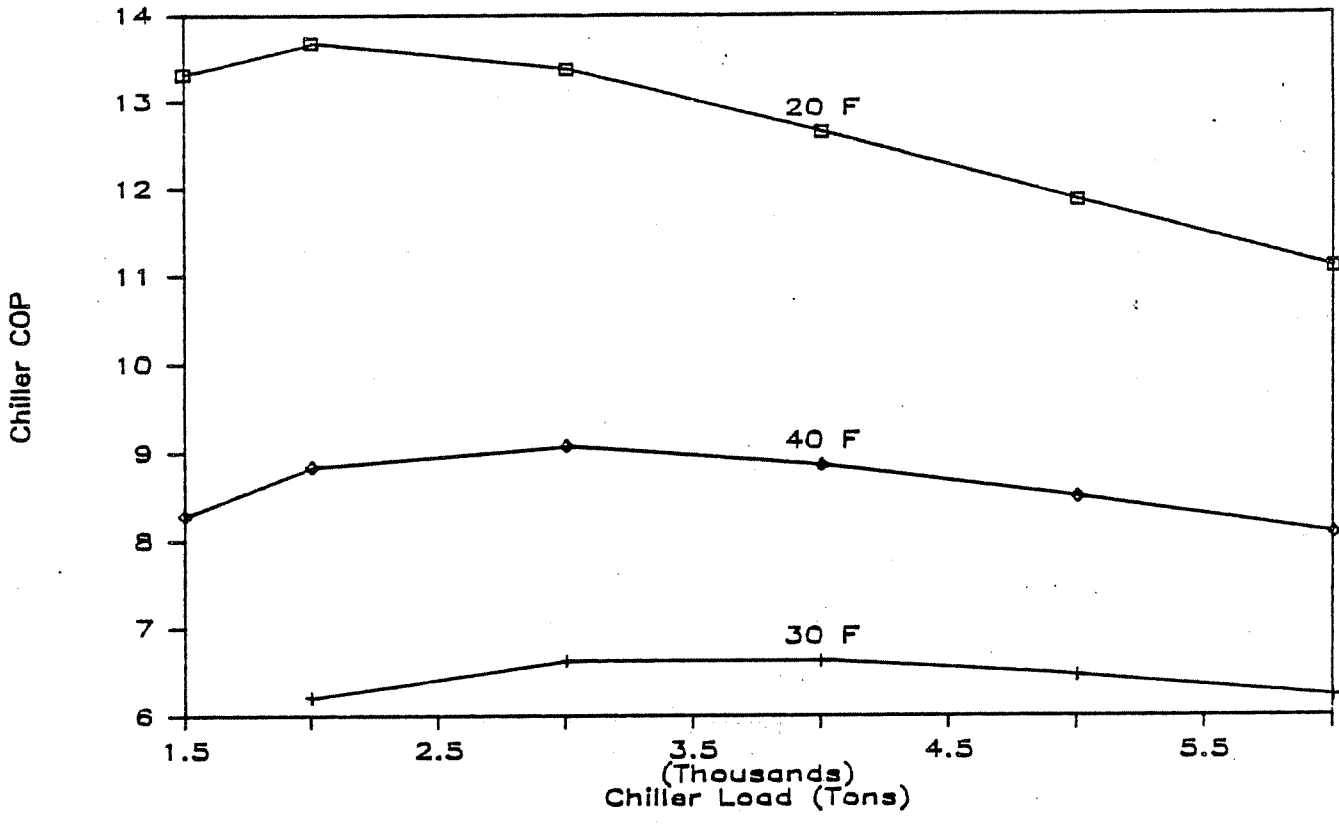


Figure 11. Modeled D/FW chiller COP vs. load requirement and leaving water temperature difference

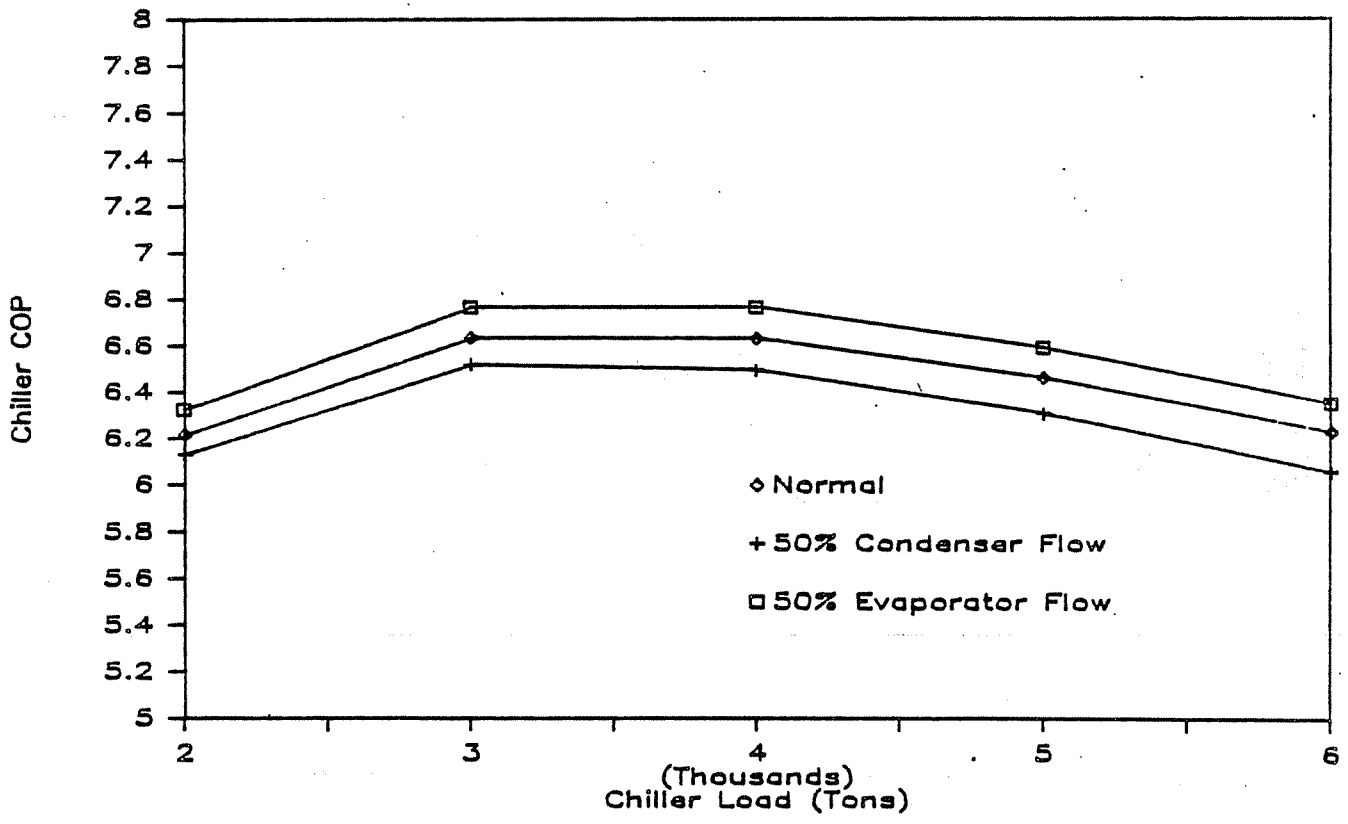


Figure 12. The effect of evaporator and condenser water flow rates on chiller COP for a fixed leaving water temperature difference of 40 F

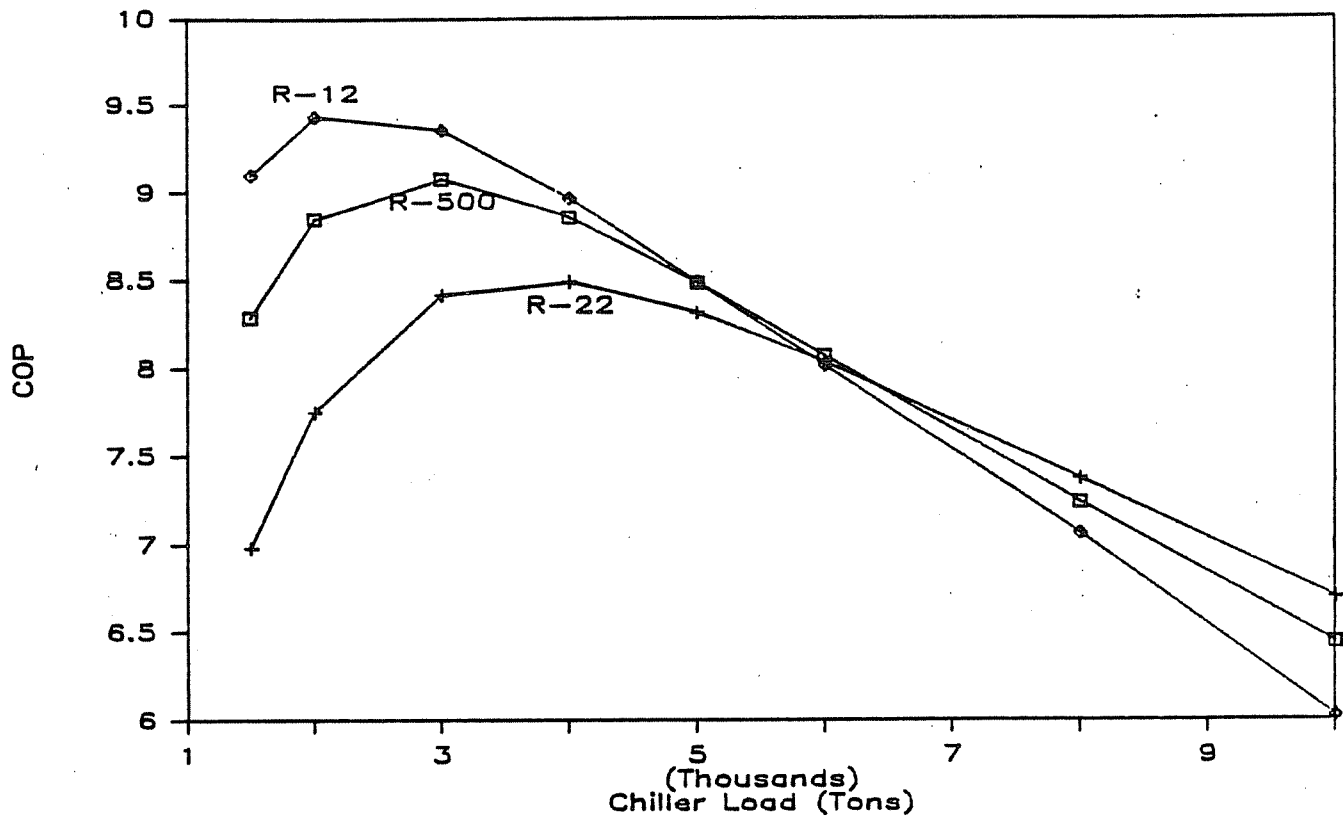


Figure 13. Comparison between refrigerant types for a leaving water temperature difference of 30 F

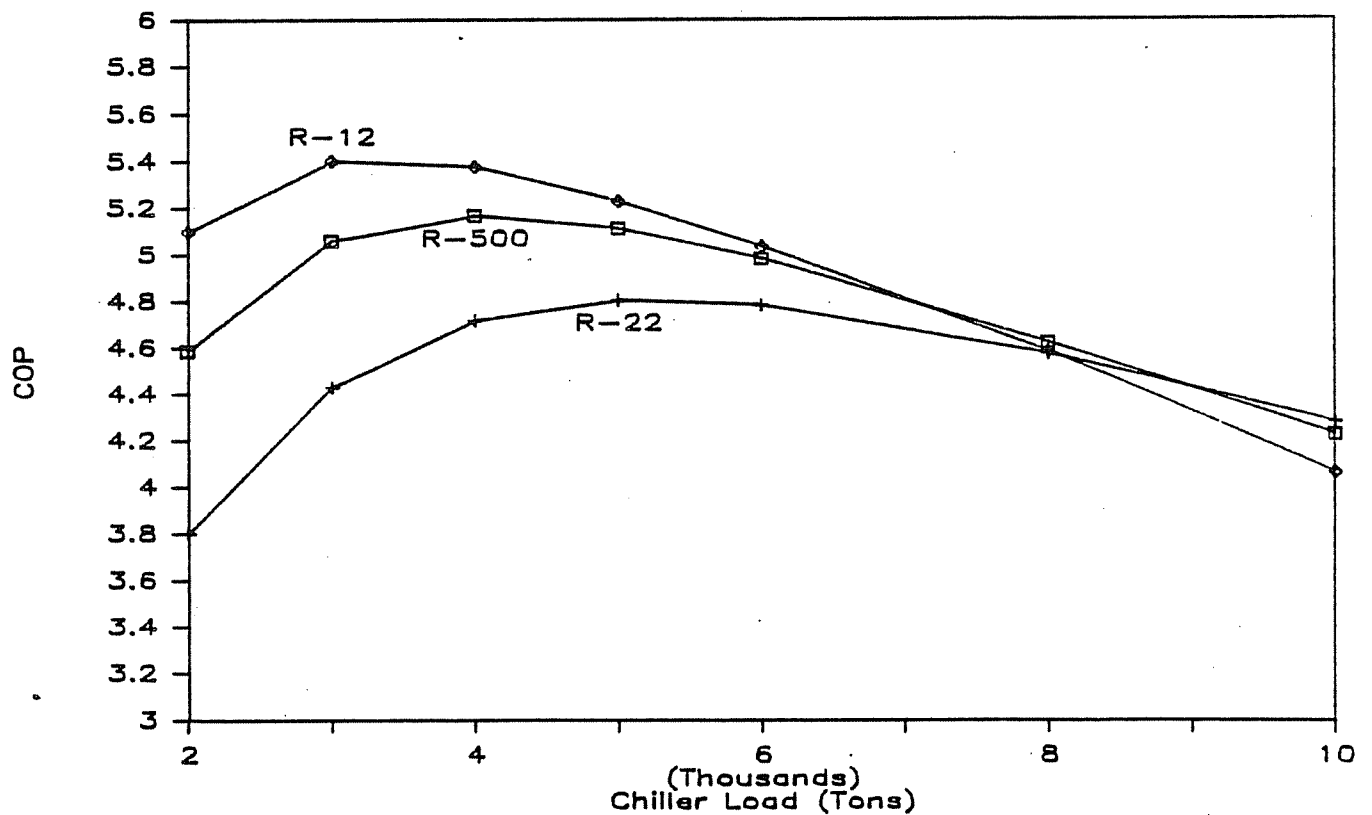


Figure 14. Comparison between refrigerant types for a leaving water temperature difference of 50 F

